Journal of Alloys and Compounds 900 (2022) 163383

Contents lists available at ScienceDirect

Journal of Alloys and Compounds

journal homepage: www.elsevier.com/locate/jalcom

On the relationship between microstructure and residual stress in laser-shock-peened Ti-6Al-4V

Sergey Mironov[a,*], Maxim Ozerov[a], Alexander Kalinenko[a], Nikita Stepanov[a], Oleg Plekhov[b], Ruslan Sikhamov[c], Volker Ventzke[c], Nikolai Kashaev[c], Gennady Salishchev[a], Lee Semiatin[d], Sergey Zherebtsov[a]

[a] Belgorod National Research University, Belgorod 308015, Russia
[b] Institute of Continuous Media Mechanics, Ural Branch of Russian Academy of Science, Perm 614013, Russia
[c] Department of Laser Processing and Structural Assessment, Institute of Materials Mechanics, Helmholtz-Zentrum Hereon, Max-Planck-Str. 1, 21502 Geesthacht, Germany
[d] Air Force Research Laboratory, Materials and Manufacturing Directorate (ret'd), Wright-Patterson AFB, OH 45433–7817, USA

ARTICLE INFO

Article history:
Received 19 October 2021
Received in revised form 30 November 2021
Accepted 20 December 2021
Available online 23 December 2021

Keywords:
Ti-6Al-4 V
Laser shock peening (LSP)
Microstructure
Residual stress
Electron backscatter diffraction (EBSD)
Transmission electron microscopy (TEM)

ABSTRACT

The relationship between residual stress and microstructure evolution during laser shock peening (LSP) of Ti-6Al-4V was investigated. To this end, the program material was processed using a 5-J Q-switched Nd:YAG laser with a wavelength of 1064 nm and a pulse duration of 20 ns. The residual stresses developed during LSP were determined by means of the incremental-hole-drilling method, and the corresponding microstructures were established using electron backscatter diffraction (EBSD) and transmission electron microscopy (TEM). From these observations, it was deduced that deformation and the resulting microstructure evolution during LSP were controlled by an inhibition of dislocation cross-slip, which, in turn, was attributed to the extremely short duration of the process. Hence, it was surmised that the unique residual-stress state generated during LSP is associated with two intrinsic characteristics of this technique, i.e., the very high imposed energy and the extremely short time scale. The large and non-uniform mechanical energy input gives rise to the residual stresses while the limited time span prevents stress relief via dislocation cross slip and climb.

1. Introduction

Due to its excellent combination of low density and high strength, Ti-6Al-4V is widely used in the aerospace industry [1]. In many applications, enhanced high-cycle fatigue (HCF) performance is also often desired [2]. In view of the major effect of material surface condition on HCF behavior, a number of techniques have therefore been developed to improve surface properties and fatigue resistance [3]. One recent innovation in this area has been the development of laser shock peening (LSP) [4]. In this approach, a pulsed laser beam is applied to generate a shock wave at the material surface. During propagation of the shock wave, the material experiences severe deformation at very high pressure (GPa level), ultra-high strain rate ($> 10^6$ s^{-1}), and ultra-short duration (~10 ns level). These attributes give rise to significant *compressive* residual stresses in the surface layer which are beneficial in retarding the initiation of fatigue.

To the present, most research on the LSP of Ti-6Al-4V has been focused on investigation of the residual stresses which are developed [5–41]. In these prior efforts, it has been found that the stress distribution tends to be relatively complex [34,36]. The highest compressive residual stresses are usually found in the near-surface layer, whereas the total depth of the stressed zone may extend to ~1.5 mm below the surface [7]. Furthermore, depending on the particular LSP processing conditions, the peak stress magnitude may be as high as ~800 MPa [36]. To maintain stress equilibrium, the surface compressive stresses are counterbalanced by tensile stresses below the surface [34,36]. Moreover, small compressive stresses are also sometimes observed at the face opposite to that subjected to the LSP pulse [34]. The residual-stress distribution in the *width* (transverse) direction of the laser-peened surface is also often found to be non-uniform due to the plastic-wave nature of the LSP strain [24,40]. As a result of the significant residual stresses, LSP normally results in a marked enhancement in fatigue

* Corresponding author.
E-mail address: mironov@bsu.edu.ru (S. Mironov).

https://doi.org/10.1016/j.jallcom.2021.163383
0925-8388/

properties [7–9,12,19,30,33,41–45], wear resistance [17,23,47], and surface hardness [6–9,11,16,17,23,31,33,38,43,46–48].

In contrast to residual-stress evolution and fatigue performance, the microstructural aspects of LSP of Ti-6Al-4V have attracted relatively-less attention in the literature. Among the limited microstructural studies, the formation of a nanocrystalline [25,37,43,48] or even amorphous [6] structure have been found in the narrow surface layer of LSP workpieces. In contrast, microstructure changes are usually much less pronounced beneath this surface layer. Typically, a significant density of tangled dislocations is found in both the α [8,9,48–50] and β [47,48] phases. Sometimes, shear banding is also observed [5,6,47]. In some instances, mechanical twinning in the α phase has also been noted [37,43,47–49], despite its rare occurrence in conventionally-processed Ti-6Al-4V. Stacking faults have also been found unexpectedly in the α phase despite its relatively-high stacking fault energy [25].

While significant progress has been achieved in the investigation of both residual stresses and microstructure, research to establish a possible relation between the two aspects is scarce. Therefore, the present study was undertaken to shed light on this issue. In particular, this work was based on the premise that residual stresses generated during LSP are inherently linked with the extreme and unusual deformation conditions that characterize it, i.e., very large imposed energy, ultra-high strain rate, and ultra-short duration, or conditions which would also have a large effect on microstruture evolution.

2. Material and experimental procedures

2.1. Program material

The material used in the present study was Ti-6Al-4V supplied as hot-rolled sheet of 6 mm thickness. Prior to LSP treatment, the surface of the material was mechanically polished to a mirror finish, cleaned in water, and then degreased in ethanol.

2.2. LSP treatment

Based on the previous studies [44,51–53], a particular combination of LSP parameters was selected to provide a deep layer of compressive residual stress. Specifically, LSP was performed using a Q-switched Nd:YAG laser with a wavelength of 1064 nm operated at 10 Hz and a pulse duration of 20 ns (full width at half maximum). The laser pulse energy and the spot size were set at 5 J and 1 × 1 mm^2, respectively, thus resulting in a power density of 25 GW/cm^2. A water layer (~1 mm thick) was used as the transparent confining medium, and 100-μm-thick steel foil was employed as an ablative (sacrificial) layer. The surface peening procedure was conducted using a square scanning grid aligned with the rolling and transverse directions of the initial hot-rolled sheet. A total peened area of 20 × 20 mm^2 was produced using a scan step size of 1 mm without overlap between adjacent laser spots. In addition, to establish the influence of the number of LSP cycles on residual stress and microstructure, given locations on a peened surface were subjected to either one or three laser pulses. In a second LSP variant, the ablative layer was replaced with a fresh one after each peening cycle.

2.3. Analysis of residual stress

After LSP processing, residual-stress profiles were determined using an incremental-hole-drilling method [54], utilizing the 'Prism' system of Stresstech company. This system is equipped with an optical electronic speckle pattern interferometer (ESPI) for high-quality full-field displacement-data acquisition. All measurements were performed using a rotational speed of 30,000 rpm and 0.04 mm/s feed rate. For each specimen, three holes were drilled inside the LSP'ed area. The minimum distance between the holes and the edge of the LSP-processed zone was 5 mm. A schematic diagram of the positions for the residual-stress analysis is shown in supplementary Fig. S1a. The holes were drilled using a two-fluted end mill of 2.0 mm diameter. According to ASTM standard E837–08, the maximum drilling depth was 1 mm in order to maintain satisfactory accuracy. In all cases, the two principal components of the stress tensor were determined, i.e., the normal stress along the prior rolling and transverse directions, herein denoted as σ_{RD} and σ_{TD}, respectively. Further experimental details have been reported elsewhere [55].

2.4. Microstructure observations

Microstructural observations were carried out using electron backscatter diffraction (EBSD) and transmission electron microscopy (TEM) techniques. A schematic showing the approximate locations of the microstructure observations is given in supplementary Fig. S1b. For EBSD, peened specimens were sectioned through the thickness and prepared using conventional metallographic techniques including a final long-time (24 h) vibratory polishing with colloidal silica. EBSD was conducted with an FEI Quanta 600 field-emission-gun scanning electron microscope (FEG-SEM) operated at an accelerating voltage of 20 kV and equipped with a TSL OIM™ system. To provide a comprehensive analysis of the LSP-induced microstructures, several EBSD maps with different scan step sizes were acquired for each material condition. Specifically, low-magnification (overview) maps were obtained using a scan step size of 1 μm, whereas high-resolution EBSD analysis was conducted with a scan step size of 0.2 μm. To improve the fidelity of EBSD data, grains comprising two or fewer pixels were automatically cleaned from EBSD maps using the grain-dilation option of the TSL software.

Specimens for TEM characterization were extracted at various depths, ground to ~100-μm thickness, and then electro-polished in a mixture of 600 ml methanol + 360 ml butanol + 40 ml perchloric acid at 29.5 V and − 35°C. In particular, the TEM samples provided microstructural information at depths of ~150 μm and ~550 μm from the laser peened surface. TEM observations were conducted with a JEOL JEM-2100 transmission electron microscope operated at 200 kV.

2.5. Image quality index and kernel-average misorientation

Two particular EBSD characteristics, viz., the image-quality (IQ) index and kernel average misorientation (KAM), were used for microstructure characterization. The IQ *index* is a measure of the sharpness of the Kikuchi bands in a particular diffraction pattern. It represents the sum of the pixels belonging to the Kikuchi lines in a particular digitalized Kikuchi pattern. Assuming proper preparation of the EBSD surface, IQ can serve as a qualitative measure of total dislocation density (i.e., statistically-stored dislocations plus geometrically-necessary ones, according to the terminology of Ashby [56]). Two types of representation of IQ data were used in the present work, i.e., color or grayscale. The former one provides a high sensitivity to microstructure changes, whereas grayscale maps resemble the appearance of the microstructure in optical microscopy or SEM.

The KAM metric is the average misorientation angle between a given pixel in an EBSD map and each of its neighboring pixels (excluding those misoriented above a predefined threshold, which is typically taken to be 5°). Therefore, KAM characterizes the local crystallographic rotations and hence is used as a measure of the density of geometrically-necessary dislocations (or equivalent local strain). In this work, the KAM measurements were conducted using the standard option of the EBSD software.

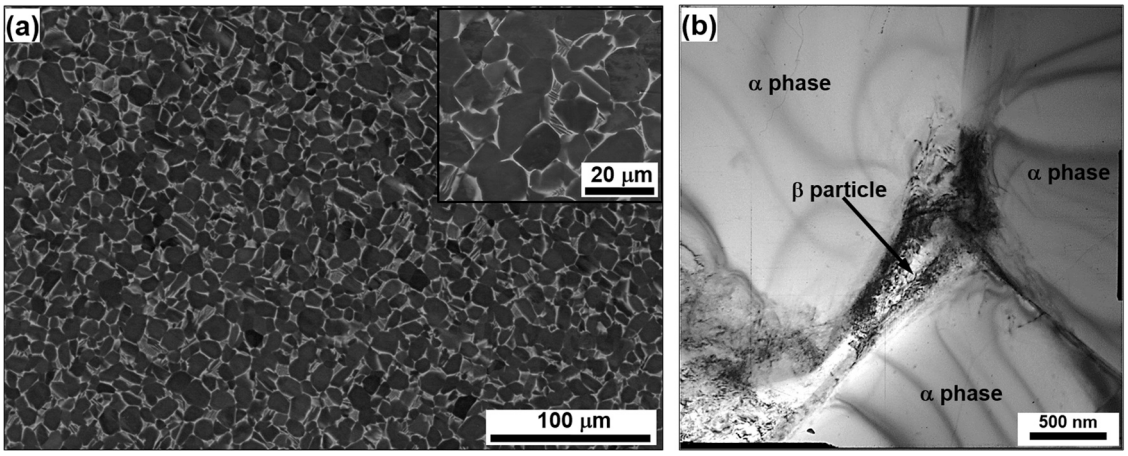

Fig. 1. Microstructure of initial material: (a) SEM image (high magnification insert is given in the top right corner) and (b) TEM micrograph. In (a), the α phase is dark, and the β phase is bright.

3. Results

3.1. Initial microstructure

In the as-received condition, the Ti-6Al-4V program material had a duplex microstructure consisting of a large fraction of globular primary α and a smaller fraction of transformed β (Fig. 1a). The average size of the primary α particles was ~10 μm, whereas

the mean thickness of the α lamellae within the transformed phase was ~0.5 μm. Furthermore, the primary α contained a relatively-low dislocation density (Fig. 1b).

3.2. Residual-stress analysis

The as-received material exhibited ascertainable tensile residual stresses in the surface layer (Fig. 2). This condition may have originated from interface friction and/or non-uniform deformation during hot rolling or was an artefact associated with the prior mechanical-polishing procedure used to fabricate the LSP test specimens.

After LSP, the residual-stress patterns were quite different (Fig. 2). As expected, they showed compressive residual stresses in the surface layer as deep as ~1 mm. In all cases, the profiles were broadly similar to each other, i.e., a relatively-low stress immediately beneath the surface, a broad peak at depths of ~200–700 μm, and a reduction in stress further into the depth. A possible origin of such stress profiles is discussed in Section 4.4. The residual-stress analysis also revealed a noticeable difference between two principal stress components (i.e., Fig. 2a vs b). This anisotropy has been described in the literature [57,58], and is usually attributed to either the asymmetry of LSP treatment or crystallographic texture in the starting material.

The magnitude of the residual-stress profiles was noticeably greater after the application of three LSP cycles (Fig. 2). In fact, the peak stresses in such instances approached ~800 MPa, thus comprising ~80% of the yield strength. At such stress levels, however, the experimental error in incremental-hole-drilling measurements tends to be relatively-high [59]. Nevertheless, considering the relatively-good reproducibility of the experimental data (Fig. 2a vs b), the accuracy of the measurements was surmised to be good. From the residual-stress analysis, it is also worth noting that the propagation depth of the LSP-induced *elastic* strain exceeded 1 mm.

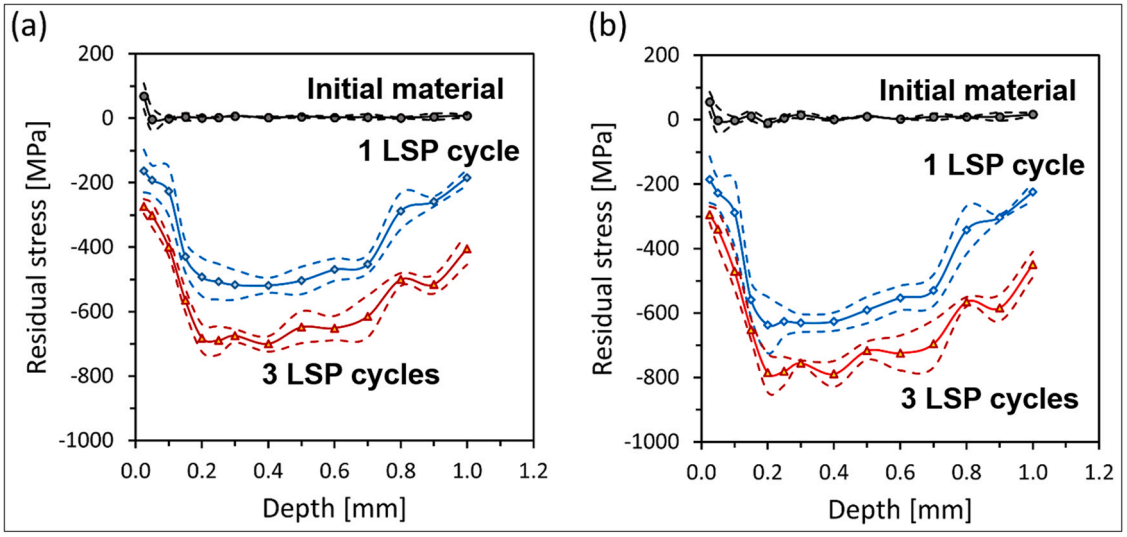

Fig. 2. Residual-stress profiles obtained using the incremental-hole-drilling method: (a) σ_{RD} component and (b) σ_{TD} component. In all cases, broken lines indicate the standard deviation of measurements.

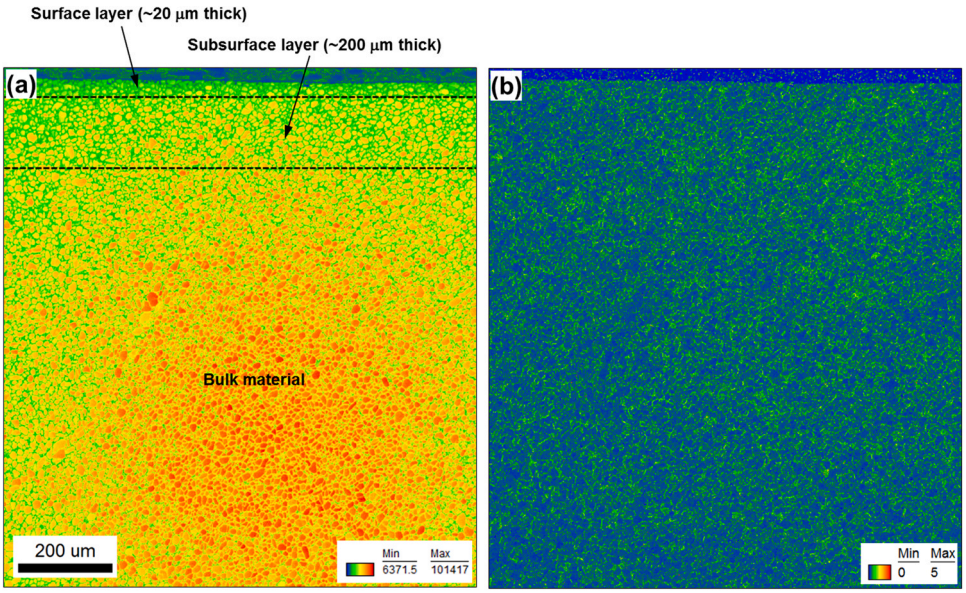

Fig. 3. Low-magnification EBSD maps which highlight different microstructural aspects after 1 LSP cycle: (a) Color-coded IQ map and (b) KAM map. The laser-peened surface is at the top. In both maps, the appropriate color code is given in the bottom right corner. In (a), the dotted lines indicate three different microstructural regions produced during LSP, i.e., surface layer, subsurface layer, and the bulk material. Note: The scale bar for both figures is given at the bottom left corner of (a). Also, the color code in (a) shows a variation of the image-quality index, which may serve as a measure of the level of local defects in the crystal structure (see Section 2.5).

3.3. EBSD examination of the peened material

3.3.1. Low-magnification EBSD results

Low-resolution (overview) EBSD maps taken from the as-processed specimens (Figs. 3 and 4) provided broad insight into microstructure evolution during LSP. In all cases, the laser-peened surface is at the top.

After a single LSP pass, three distinct microstructural regions were noted in the IQ map (Fig. 3a), viz., a narrow (~20 μm thick) surface layer, a wider (~200 μm thick) subsurface zone, and an apparently-unaffected (bulk-microstructure) area. Not surprisingly, the surface layer with the highest deformation/dislocation density was characterized by the lowest image-quality index. On the other hand, the KAM measurements revealed no noticeable anomalies near the laser-peened surface (Fig. 3b).

Three LSP cycles resulted in a marked increase in the depth of the surface layer (i.e., Figs. 3a vs. 4a) and the development of noticeable surface undulations (Fig. 4a). The latter behavior follows previously-reported observations [7,11,33,47], and is sometimes attributed to the non-uniform distribution of the shock pressure induced during LSP [47]. This observation is discussed in the following section. The KAM map after 3 LSP cycles also revealed the formation of a distinct heavy-deformation zone near the peened surface (Fig. 4b). Assuming that IQ and KAM metrics may serve as characteristics of dislocation

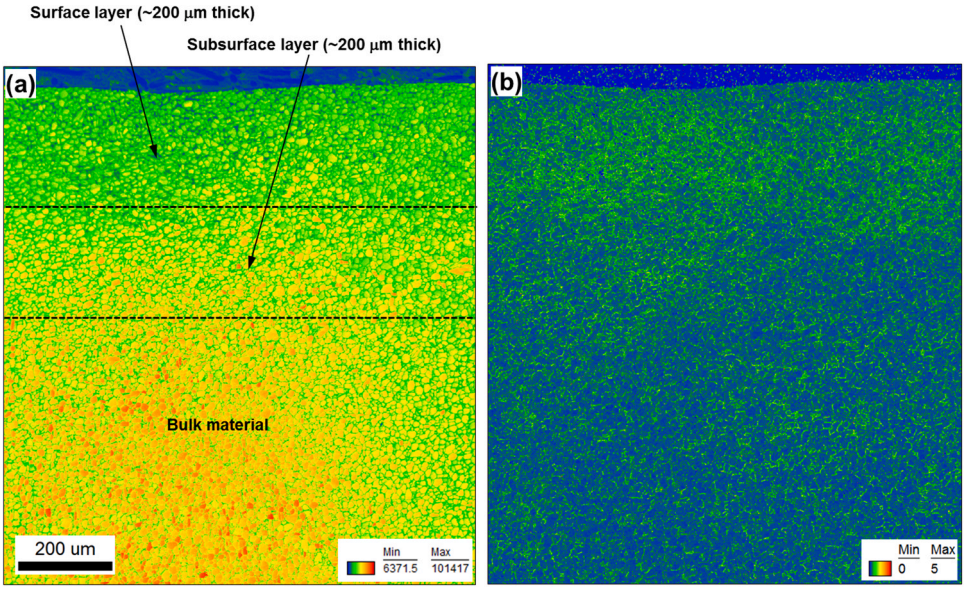

Fig. 4. Low-magnification EBSD maps which highlight different microstructural aspects after 3 LSP cycles: (a) Color-coded IQ map and (b) KAM map. The laser-peened surface is at the top. In both maps, the appropriate color code is given in the bottom right corner. In (a), the dotted lines indicate three different microstructural regions produced during LSP, i.e., surface layer, subsurface layer, and bulk material. Note: The scale bar for both figures is given at the bottom left corner of (a). Also, the color code in (a) shows a variation of the image-quality index, which may serve as a measure of the level of local defects in the crystal structure (see Section 2.5).

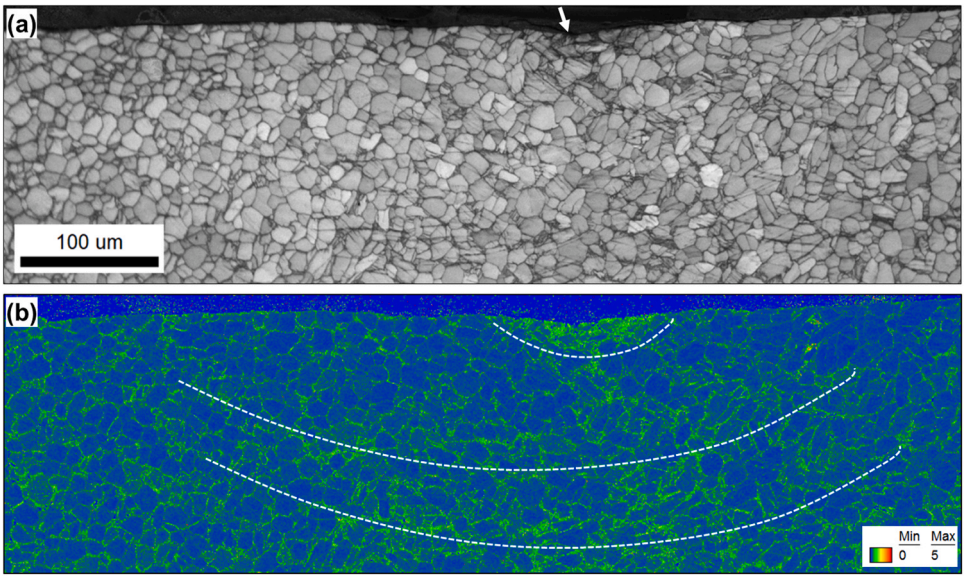

Fig. 5. High-magnification EBSD maps showing the inhomogeneous microstructure distribution directly beneath the peened surface: (a) Grayscale IQ map and (b) KAM map. The laser-peened surface is at the top. In (a), the arrow indicates the most heavily-deformed area. In (b), the dotted lines show the presumed front of shock wave propagation. The scale bar for both figures is given in the bottom left corner of (a).

structure (Section 2.5), the results shown in Fig. 4 implied a noticeable increase in dislocation density in the surface region.

It is important to note that in the both peened conditions (1 vs 3 LSP cycles), the material at a depth of 200 µm or greater from the surface was characterized by a relatively-high IQ index (Figs. 3a and 4a) but low KAM index (Figs. 3b and 4b). Per the definitions of the IQ and KAM metrics given in Section 2.5, this suggested that the bulk material exhibited only minor evidence of plastic strain. On the other hand, such locations were characterized by the highest residual stresses (Fig. 2). In other words, the microstructural observations appeared to be inconsistent with the residual-stress analysis.

3.3.2. High-resolution analysis

High-resolution EBSD maps acquired from the material subjected to 3 LSP cycles (e.g., Fig. 5) provided deeper insight into microstructural processes occurring in the surface layer. From such maps, it was evident that the peened material exhibited noticeable surface relief/undulation (a typical example is indicated by the arrow in Fig. 5a). This observation was in the line with literature data [24,40] and can be attributed to the inhomogeneous (i.e., Gaussian) distribution of energy during laser pulsing. It was likely that the laser intensity was preferentially concentrated along the optical axis of the laser beam, thus giving rise to a surface topography such as that shown in Fig. 5a.

The corresponding KAM map (Fig. 5b) was of particular interest. As mentioned in Section 2.5, the KAM metric may serve as a measure of local intra-granular strain. Hence, the specific variation of the KAM contrast in Fig. 5b appeared to indicate that highly-strained grains tended to cluster together, yielding what appeared to be extended wave-shaped domains (indicated by the dotted lines in Fig. 5b). Those domains were intermixed with layers of grains which apparently had little to no strain. EBSD measurements on the initial material revealed the remnants of a colony-α structure (supplementary Fig. S2) but no distinct microstructural banding (i.e., alternating layers with higher and lower Taylor factors), which could give rise to such a specific deformation distribution near the laser-peened surface (supplementary Fig. S3). To a first approximation, therefore, the microstructural pattern revealed in Fig. 5b may be indicative of the propagation front of the shock wave induced during LSP.

Although the wave-like nature of LSP straining is sometimes implied (or postulated) in the LSP literature [e.g., 9–11], clear microstructural evidence of this phenomenon has not heretofore been provided to the best of the authors' knowledge. On the other hand, it should be emphasized that the wave-shaped domains in Fig. 5b are not obvious, and therefore the above suggestion is still speculative and warrants further study.

3.3.3. Micro-mechanisms of LSP strain

High-resolution EBSD maps acquired directly beneath the laser indent (Fig. 6a) provided insight into the *micro-mechanisms* of LSP strain. It was found that the α particles in this area often contained lenticular- or wedge-shaped features delineated by $85^{o} < 2\bar{1}\bar{1}0>$ boundaries (red lines in Fig. 6a). This observation implied the activation of $\{10\bar{1}2\} < \bar{1}011>$ twinning in the α phase during LSP, thus being in the line with some prior observation [37,43,47–49].

In addition to twinning, high-resolution EBSD also revealed narrow dark-contrast bands within α particles (Fig. 6a). These bands typically extended across entire particles and were often arranged in nearly-parallel series, thus subdividing the original particles into a block-type substructure. Such microstructures have also been reported before in the literature as being attributable to the occurrence of deformation banding [5,6,47]. In the present study, the observation that the band traces were typically (although not always) close to traces of $\{10\bar{1}0\}$ slip planes (dotted lines in Fig. 6a) was of particular interest. This result may indicate a prevalence of conventional prism slip (i.e., the easiest slip mode in α titanium) during LSP. It is worth noting, however, that the boundary alignment was not entirely conclusive in characterizing slip activity, and therefore additional (texture) analysis is needed to support to the above suggestion.

It is also important to emphasize that the misorientation across the deformation-band boundaries was typically below 2° (i.e., the EBSD resolution limit), as exemplified by the misorientations profiles (red lines) in Fig. 6b and c.[1] Considering the very high energy imposed during laser pulsing (25 GW/cm^2), such misorientations seem to be surprisingly low. In this context, it is also noteworthy that the formation of a nanocrystalline structure has also been reported

[1] A total of 18 misorientation profiles were measured in the present study (supplementary Fig. S4).

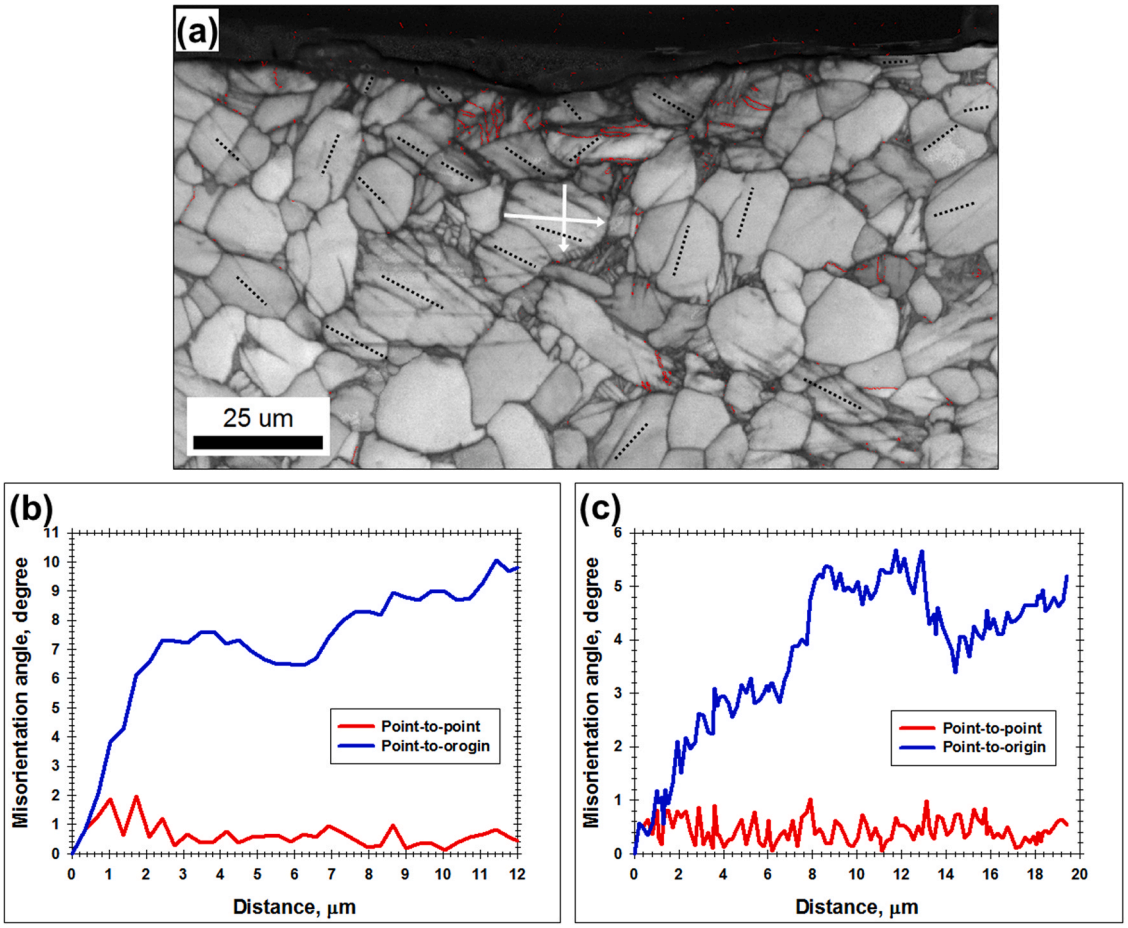

Fig. 6. High-resolution EBSD analysis of a heavily-deformed area: (a) Grayscale IQ map, (b) misorientation profile measured along the vertical white arrow shown in (a), and (c) misorientation profile measured along the horizontal white arrow shown in (a). In (a), the laser peened surface is at the top, the red lines indicate 85° < 2–1–10 > twin boundaries, the black dotted lines show the traces of {10–10} slip planes which are closest to the orientation of deformation bands, and the white arrows are the misorientation profiles given in (b) and (c), respectively.

in some previous efforts at noticeably lower laser-power density (11.89 GW/cm^2) [25,37,43].

Despite the low misorientations across the deformation bands, LSP did give rise to large grain-scale orientation gradients, as indicated by the blue lines in Fig. 6b and c). The magnitude of such gradients corresponded to ~1°/μm (Fig. 6b), thus being relatively high. These gradients presumably reflected a substantial variation in slip activity at the grain scale. Strain inhomogeneity was also evidenced by the fact that the orientation gradients were typically larger in the depth direction compared to those in the transverse direction (Fig. 6b vs. c).

3.3.4. Nature of slip activity

The IQ and KAM distributions derived from EBSD provided yet further insight into the dislocation processes occurring in the surface layer during LSP. The measurements revealed broadly similar trends in both the α and β phases. Therefore, the results for the α phase only are presented herein (Fig. 7), while those for the β phase are given in supplementary Fig. S5. Per the data in Fig. 7a, LSP gave rise to a gradual shifting of the IQ distribution toward lower values. This observation can be attributed to an increase in total dislocation density with increasing number of LSP cycles.

On the other hand, the KAM measurements revealed only subtle changes (Fig. 7b). Assuming that the KAM metric characterizes local crystallographic rotations (Section 2.5), the data shown in Fig. 7b virtually suggested relatively-little activity of geometrically- necessary dislocations. Hence, it can be surmised that LSP preferentially generated statistically-stored dislocations.

3.4. TEM observations of peened material

TEM examinations in proximity to the peened surface (Fig. 8) gave a closer look into LSP-induced dislocation processes. Deformation behavior during the early stage of LSP was deduced from observations at a relatively large material depth (~550 μm) in a specimen subjected to a single LSP cycle. Here, the dominant substructure comprised planar arrays of dislocations (Fig. 8a). Approaching the peened surface (and thus regions with higher imposed strains), the planar dislocation arrays transformed to deformation bands (Fig. 8b) similar to those seen in EBSD maps (Fig. 6a). Selected-area-diffraction patterns taken from both the banded and the matrix regions (e.g., top right corner of Fig. 8b) revealed very small orientation differences across the bands. This finding also agreed well with the EBSD results discussed in Section 3.3.3.

TEM observations for specimens subjected to *three* LSP cycles were also consistent with EBSD measurements. In particular, the microstructure distribution was fairly inhomogeneous including both apparently strain-free grains (Fig. 8c) and heavily-deformed grains (Fig. 8d to f). In the latter case, a series of dislocation boundaries (Fig. 8e) and mechanical twins (Fig. 8 f) were found. The typical dislocation structure in this case consisted of dislocation tangles (Fig. 8d), thus contrasting to the dislocation arrays developed during a single LSP pass. This observation presumably implied the

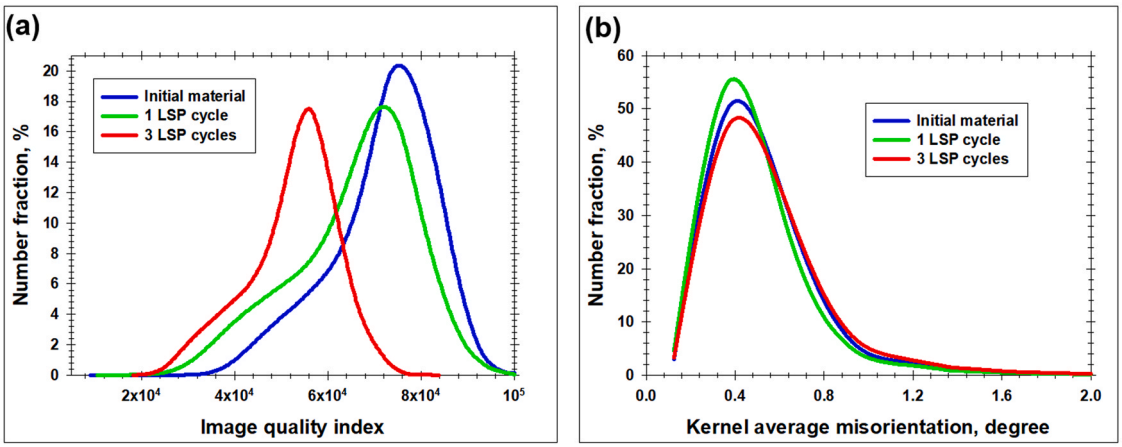

Fig. 7. Effect of LSP on (a) IQ index and (b) KAM in the α phase in the surface layer of the peened material.

activation of multiple slip as well as a marked difficulty of cross slip. In this regard, high densities of tangled dislocations are typically observed in LSP-processed Ti-6Al-4V [8,9,47–50].

From the TEM observations, it is clear that the LSP-induced microstructure varied from dense dislocation boundaries and mechanical twins near the surface of the pulsed specimens (Fig. 8e and f, respectively) to poorly-developed planar dislocation arrays in the bulk material (Fig. 8a). This gradient implies a complex character of microstructural development during LSP.

4. Discussion

4.1. Broad aspects of LSP-induced residual stress

To understand the deformation behavior during LSP, it is important to realize that the temporal duration of such a treatment is extremely short. Specifically, the duration of the laser pulse employed in the present work was 10^{-8} s^{-1}. Assuming a plastic-wave-type character of strain propagation (as discussed in Section 3.3.2)

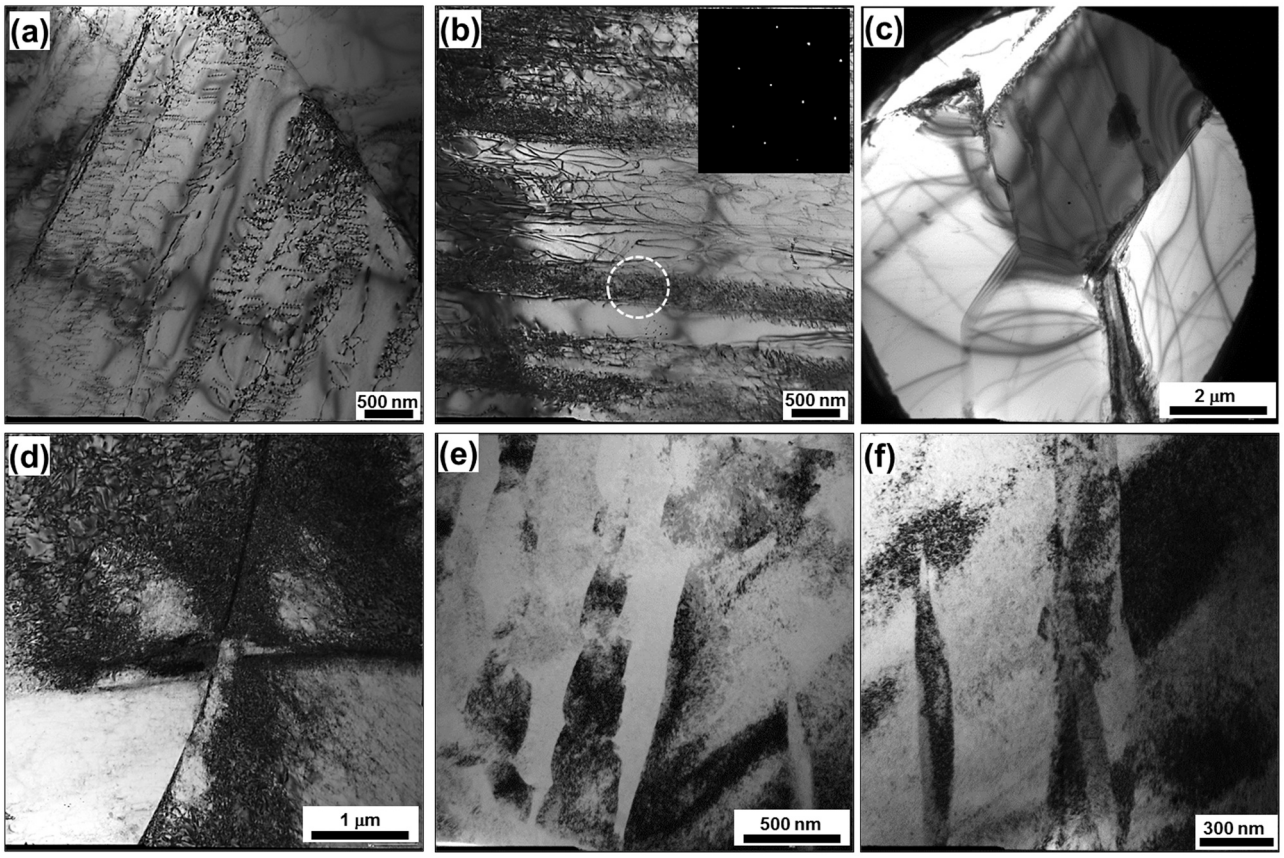

Fig. 8. TEM micrographs showing characteristic microstructures observed in LSP'ed material: (a) Planar dislocation arrays (1 LSP cycle), (b) deformation bands (with the selected-area-diffraction pattern shown in the top right corner) (1 LSP cycle), (c) dislocation-free grains (3 LSP cycles), (d) dislocation tangles (3 LSP cycles), (e) dislocation boundaries (3 LSP cycles), and (f) mechanical twins (3 LSP cycles). In (a), the micrographs were taken at a depth of ~550 μm from the peened surface; in the other cases, the observation depth was ~150 μm. In (b), the area from which the diffraction pattern was taken is circled.

and assuming a maximum wave speed equal to the speed of sound (~3000 to 6000 m/s in titanium), the characteristic propagation time of the wave across the specimen thickness was ~10^{-6} s^{-1}. In view of this timescale, it seems unlikely that LSP deformation processes would involve any diffusion-assisted mechanisms.

The precise mechanism of the absorption of the laser-pulse energy by a workpiece material is not completely clear. From a broad perspective, it may involve both a thermal effect as well as the shock strain itself. Due to the exceptionally short duration of LSP, the essentially-adiabatic heating transient is difficult to measure experimentally. In the present study, no any evidence of material heating was found. Moreover, the relatively-high density of tangled dislocations (Fig. 8d to f) suggested a relatively-low processing temperature. It was hypothesized, therefore, that the residual stress originated from mechanical impact rather than from a temperature gradient.

Conventionally, residual stresses can be broadly classified into two types depending on their range of influence, i.e., macro-scale and micro-scale. In the present research, the *sample-scale* stresses were apparently associated with the inhomogeneous strain distribution developed throughout the thickness of the peened sample. On the other hand, *grain-scale* stresses are usually related to strain incompatibility between neighboring grains (or phases). Such stresses are linked directly to the specific microstructure produced within deformed grains. Hence, these were of particular interest in the present study.

4.2. Micro-scale stress

In this work, the microstructural characteristics of peened Ti-6Al-4V specimens included (i) a prevalence of planar- or tangled- dislocation structures (Fig. 8), (ii) a relatively-low activity of geometrically-necessary dislocations (Fig. 7b) with a concomitant orientation spread (Fig. 6b, c), and (iii) very slow kinetics of evolution of dislocation boundaries (Figs. 6b, c and 8b). Each of these observations can be explained on the basis of limited cross slip during LSP deformation. Specifically, the lack of cross slip should prevent redistribution of free dislocations into dislocation boundaries, inhibit the progressive evolution of such boundaries toward high misorientations, and thus suppress the relief of grain-scale stresses.

As cross slip is a diffusion-controlled process, it should depend critically on the duration of the processing treatment. Hence, its activation appears to be difficult under the deformation conditions characteristic of LSP.

It is thus surmised that the unique stress-state generated during LSP is associated with two intrinsic characteristics of the technique, i.e., a very high imposed energy and an extremely-short timescale. The large mechanical energy gives rise to the stresses within the processed material whereas the very short duration of LSP tends to prevent their relief via dislocation cross slip and climb.

4.3. The possible influence of the wave-type nature of LSP strain

Although the wave-like nature of LSP straining still warrants additional experimental verification, its possible influence on microstructure evolution is briefly discussed here. Assuming a wave character of strain propagation, the material beneath a particular laser spot should be influenced by the deformation induced by neighboring laser indents. Moreover, due to the circular geometry of the strain-propagation front (and the concomitant orientation change of the shock wave), this additional strain may thus activate additional slip systems. This simple idea can be used to rationalize the transformation of dislocation pile-ups into dislocation tangles (Fig. 8a and d, respectively) observed in the present study. On the other hand, considering the very limited timescale of each LSP pass, any interaction of neighboring shock waves seems unlikely, i.e. the time span of neighboring pulses should not overlap. Hence, the wave nature of the LSP strain can be concluded to result in a sequence of several short-deformation events rather than a single deformation process. If so, the wave mechanism of strain propagation should not enhance the occurrence of cross slip.

4.4. Macro-scale stress

The residual-stress profiles observed in the present study were characterized by a relatively-low magnitude at the surface (Fig. 2) and substantially-higher (peak) levels outside the most heavily-deformed surface region (compare Figs. 2 and 4). Such residual-stress patterns with a subsurface peak are often found in LSP-processed Ti-6Al-4V [16,26,28,34,42,44,53,57,58]. On the other hand, there have also been a number of efforts in which the peak residual stresses were located directly at the surface of the peened material [5–7,9,10,13,23,25,27,30,37,38,41,42,48]. The reason for this discrepancy is not clear, and obviously warrants additional study.

Assuming that the present residual-stress analysis is reliable, it may be hypothesized that the trends observed here are associated with some form of stress redistribution due to spatio-temporal variations in plastic strain, non-uniform elastic unloading, etc. The situation is further complicated by the two- (or three-) dimensional wave-like nature of both plastic straining and elastic unloading. Such complications mandate the use of an advanced dynamic plasticity (hydro) code and detailed constitutive model to predict residual-stress patterns, however.

5. Summary and conclusions

The relationship between microstructure and residual stress produced during LSP of Ti-6Al-4V was investigated using a Nd:YAG laser operated with a wavelength of 1064 nm, a pulse duration of 20 ns, and a laser intensity of 25 GW/cm^2. The resulting distributions of (surface/near surface) compressive residual stresses were quantified using the incremental-hole-drilling method, and microstructures were determined using EBSD and TEM techniques. The main conclusions derived from this work are as follows.

(1) Microstructural analysis suggests that LSP-induced deformation is characterized by limited cross slip and climb of dislocations associated with the extremely short timescale of the process. In addition, it can be surmised that the unique residual-stress state generated during LSP is associated with two intrinsic characteristics of this technique, i.e., the very high imposed energy and extremely short timescale. The large mechanical energy gives rise to the stresses within the processed material whereas the very short duration of LSP prevents stress relief via dislocation cross-slip.
(2) LSP-processed material contains $\{10\bar{1}2\}$ twins and poorly-developed dislocation boundaries whose traces often lay close those for $\{10\bar{1}0\}$ slip planes. From these observations, it is concluded that the plastic strain imposed during LSP is accommodated by twinning and prism slip.
(3) EBSD KAM measurements reveal a very specific dislocation structure is developed during LSP, i.e., grains with relatively-high dislocation density clustered together in extended wave-shaped domains and layers of apparently dislocation-free grains. This microstructural pattern mirrors the geometry of the wave-propagation front imparted during LSP.

CRediT authorship contribution statement

S. Mironov: Conceptualization, Formal analysis, Data curation, Investigation, Methodology, Software, Visualization, Writing –

original draft preparation. **M. Ozerov:** Investigation, Methodology, Writing – review and editing. **A. Kalinenko:** Investigation, Methodology, Writing – review and editing. **N. Stepanov:** Writing – review and editing. **O. Plekhov:** Conceptualization, Funding acquisition, Writing – review and editing. **R. Sikhamov:** Investigation, Methodology, Software, Visualization, Writing – review and editing. **V. Ventzke:** Writing – review and editing. **N. Kashaev:** Conceptualization, Formal analysis, Data curation, Writing - review & editing. **G. Salishchev:** Conceptualization, Writing – review and editing. **S.L. Semiatin:** Conceptualization, Writing – review and editing. **S. Zherebtsov:** Conceptualization, Project administration, Supervision, Writing – review and editing.

Declaration of Competing Interest

The authors declare that they have no known competing financial interests or personal relationships that could have appeared to influence the work reported in this paper.

Acknowledgments

Financial support from the Russian Fund for Fundamental Research (project No. 20–48-596005) is gratefully acknowledged. The authors also would like to thank the personnel of the Joint Research Center “Technology and Materials” at Belgorod State National Research University for assistance with the microstructural observations.

Appendix A. Supporting information

Supplementary data associated with this article can be found in the online version at doi:10.1016/j.jallcom.2021.163383.

References

[1] R.R. Boyer, An overview on the use of titanium in the aerospace industry, Mater. Sci. Eng. A 213 (1996) 103–114, https://doi.org/10.1016/0921-5093(96)10233-1
[2] R. Wanhill, S. Barter, L. Molent, Fatigue Crack Growth Failure And Lifting Analysis For Metallic Aircraft Structures And Components, Springer Nature B.V.,, Dordrecht, the Netherlands, 2019.
[3] M. Sticchi, D. Schnubel, N. Kashaev, N. Huber, Review of residual stress modification techniques for extending the fatigue life of metallic aircraft components, Appl. Mech. Rev. 67 (2015) 010801, https://doi.org/10.1115/1.4028160
[4] C.S. Montross, T. Wei, L. Ye, G. Clark, Y.-W. Mai, Laser shock processing and its effects on microstructure and properties of metal alloys: A review, Int. J. Fatigue 24 (2002) 1021–1036, https://doi.org/10.1016/S0142-1123(02)00022-1
[5] S.J. Laine, K.M. Knowles, P.J. Doorbar, R.D. Cutts, D. Rugg, Microstructural characterisation of metallic shot peened and laser shock peened Ti–6Al–4V, Acta Mater. 123 (2017) 350–361, https://doi.org/10.1016/j.actamat.2016.10.044
[6] X. Pan, W. He, X. Huang, X. Wang, X. Shi, W. Jia, L. Zhou, Plastic deformation behavior of titanium alloy by warm laser shock peening: Microstructure evolution and mechanical properties, Surf. Coat. Technol. 405 (2021) 126670, https://doi.org/10.1016/j.surfcoat.2020.126670
[7] R.K. Nalla, I. Altenberger, U. Noster, G.Y. Liu, B. Scholtes, R.O. Ritchie, On the influence of mechanical surface treatments—deep rolling and laser shock peening—on the fatigue behavior of Ti–6Al–4V at ambient and elevated temperatures, Mater. Sci. Eng. A 355 (2003) 216–230, https://doi.org/10.1016/S0921-5093(03)00069-8
[8] I. Altenberger, R.K. Nalla, Y. Sano, L. Wagner, R.O. Ritchie, On the effect of deep-rolling and laser-peening on the stress-controlled low- and high-cycle fatigue behavior of Ti–6Al–4V at elevated temperatures up to 550°C, Int. J. Fatig. 44 (2012) 292–302, https://doi.org/10.1016/j.ijfatigue.2012.03.008
[9] X.C. Zhang, Y.K. Zhang, J.Z. Lu, F.Z. Xuan, Z.D. Wang, S.T. Tu, Improvement of fatigue life of Ti–6Al–4V alloy by laser shock peening, Mater. Sci. Eng. A 527 (2010) 3411–3415, https://doi.org/10.1016/j.msea.2010.01.076
[10] A. King, A. Steuwer, C. Woodward, P.J. Withers, Effects of fatigue and fretting on residual stresses introduced by laser shock peening, Mater. Sci. Eng. A 435–436 (2006) 12–18, https://doi.org/10.1016/j.msea.2006.07.020
[11] Y.B. Guo, R. Caslaru, Fabrication and characterization of micro dent arrays produced by laser shock peening on titanium Ti–6Al–4V surfaces, J. Mater. Proc. Technol. 211 (2011) 729–736, https://doi.org/10.1016/j.jmatprotec.2010.12.007
[12] S. Spanrad, J. Tong, Characterisation of foreign object damage (FOD) and early fatigue crack growth in laser shock peened Ti–6Al–4V aerofoil specimens, Mater. Sci. Eng. A 528 (2011) 2128–2136, https://doi.org/10.1016/j.msea.2010.11.045
[13] Z. Zhou, S. Bhamare, G. Ramakrishnan, S.R. Mannava, K. Langer, Y. Wen, D. Qian, V.K. Vasudevan, Thermal relaxation of residual stress in laser shock peened Ti–6Al–4V alloy, Surf. Coat. Technol. 206 (2012) 4619–4627, https://doi.org/10.1016/j.surfcoat.2012.05.022
[14] K. Ding, FEM simulation of two sided laser shock peening of thin sections of Ti-6Al-4V alloy, Surf. Eng. 19 (2003) 127–133, https://doi.org/10.1179/026708403225002568
[15] S. Zabeen, M. Preuss, P.J. Withers, Evolution of a laser shock peened residual stress field locally with foreign object damage and subsequent fatigue crack growth, Acta Mater. 83 (2015) 216–226, https://doi.org/10.1016/j.actamat.2014.09.032
[16] J. Lu, H. Lu, X. Xu, J. Yao, J. Cai, K. Luo, High-performance integrated additive manufacturing with laser shock peening –induced microstructural evolution and improvement in mechanical properties of Ti6Al4V alloy components, Int. J. Mach. Tools Manuf. 148 (2020) 103475, https://doi.org/10.1016/j.ijmachtools.2019.103475
[17] D. Kumar, S.N. Akhtar, A.K. Patel, J. Ramkumar, K. Balani, Tribological performance of laser peened Ti–6Al–4V, Wear 322–323 (2015) 203–217, https://doi.org/10.1016/j.wear.2014.11.016
[18] P.R. Smith, M.J. Shepard, P.S. Prevey III, A.H. Clauer, Effect of power density and pulse repetition on laser shock peening of Ti-6Al-4V, J. Mater. Eng. Perform. 9 (2000) 33–37, https://doi.org/10.1361/105994900770346259
[19] S.D. Cuellar, M.R. Hill, A.T. DeWald, J.E. Rankin, Residual stress and fatigue life in laser shock peened open hole samples, Int. J. Fatigue 44 (2012) 8–13, https://doi.org/10.1016/j.ijfatigue.2012.06.011
[20] S. Zabeen, M. Preuss, P.J. Withers, Residual stresses caused by head-on and 45° foreign object damage for a laser shock peened Ti–6Al–4V alloy aerofoil, Mater. Sci. Eng. A 560 (2013) 518–527, https://doi.org/10.1016/j.msea.2012.09.097
[21] Y. Cao, Y.C. Shin, B. Wu, Parametric study on single shot and overlapping laser shock peening on various metals via modeling and experiments, J. Manuf. Sci. Eng. 132 (2010) 061010, https://doi.org/10.1115/1.4002850
[22] S. Spanrad, J. Tong, Characterization of foreign object damage (FOD) and early fatigue crack growth in laser shock peened Ti-6AL-4V aerofoil specimens, Proc. Eng. 2 (2010) 1751–1759, https://doi.org/10.1016/j.proeng.2010.03.188
[23] M. Yin, Z. Cai, Z. Li, Z. Zhou, W. Wang, W. He, Improving impact wear resistance of Ti-6Al-4V alloy treated by laser shock peening, Trans. Nonfer. Met. Soc. China 29 (2019) 1439–1448, https://doi.org/10.1016/S1003-6326(19)65051-X
[24] Q. Xie, R. Li, Y.D. Wang, R. Su, J. Lian, Y. Ren, W. Zheng, X. Zhou, Y. Wang, The in-depth residual strain heterogeneities due to an indentation and a laser shock peening for Ti-6Al-4V titanium alloy, Mater. Sci. Eng. A 714 (2018) 140–145, https://doi.org/10.1016/j.msea.2017.12.073
[25] L. Lan, X. Jin, S. Gao, B. He, Y. Rong, Microstructural evolution and stress state related to mechanical properties of electron beam melted Ti-6Al-4V alloy modified by laser shock peening, J. Mater. Sci. Technol. 50 (2020) 153–161, https://doi.org/10.1016/j.jmst.2019.11.039
[26] M.J. Shepard, Laser shock processing induced residual compression: Impact on predicted crack growth threshold performance, J. Mater. Eng. Perform. 14 (2005) 495–502, https://doi.org/10.1361/105994905×56214
[27] X. Ren, B. Chen, J. Jiao, Y. Yang, W. Zhou, Z. Tong, Fatigue behavior of double-sided laser shock peened Ti-6Al-4V thin blade subjected to foreign object damage, Opt. Laser Technol. 121 (2020) 105784, https://doi.org/10.1016/j.optlastec.2019.105784
[28] N. Kalentics, A. Burn, M. Cloots, R.E. Loge, 3D laser shock peening as a way to improve geometrical accuracy in selective laser melting, Int. J. Adv. Manuf. Technol. 101 (2019) 1247–1254, https://doi.org/10.1007/s00170-018-3033-3
[29] M.P. Sealy, Y.B. Guo, Fabrication and finite element simulation of micro-laser shock peening for micro dents, Int. J. Comp. Meth. Eng. Sci. Mech. 10 (2009) 134–142, https://doi.org/10.1080/15502280802665975
[30] Y. Yang, W. Zhou, B. Chen, Z. Tong, L. Chen, X. Ren, Fatigue behaviors of foreign object damaged Ti-6Al-4V alloys under laser shock peening, Int. J. Fatigue 136 (2020) 105596, https://doi.org/10.1016/j.ijfatigue.2020.105596
[31] A.K. Gujba, L. Hackel, M. Medraj, Water droplet erosion performance of laser shock peened Ti-6Al-4V, Metals 6 (2016) 262–282, https://doi.org/10.3390/met6110262
[32] A. King, A.D. Evans, M. Preuss, P.J. Withers, C. Woodward, Study of residual stresses introduced by laser shock peening in wide chord fan blades by neutron and synchrotron diffraction, J. Neut. Res. 12 (2004) 207–211, https://doi.org/10.1080/10238160410001734694
[33] Z. Wang, Y. Jia, X. Zhang, Y. Fu, C. Zhang, S. Tu, Effects of different mechanical surface enhancement techniques on surface integrity and fatigue properties of Ti-6Al-4V: a review, Crit. Rev. Sol. St. Mater. Sci. 44 (2019) 445–469, https://doi.org/10.1080/10408436.2018.1492368
[34] J. Everaerts, X. Song, B. Nagarajan, A.M. Korsunsky, Evaluation of macro- and microscopic residual stresses in laser shock-peened titanium alloy by FIB-DIC ring-core milling with different core diameters, Surf. Coat. Technol. 349 (2018) 719–724, https://doi.org/10.1016/j.surfcoat.2018.06.043
[35] Y.J. Luo, J.B. Chen, X.F. Wang, Y.X. Zhao, A.B. Zhang, C. Xie, Y. Chen, J.K. Du, A micromechanical model to study the closure stress effect on fatigue life of Ti6Al4V subjected to laser shock peening, Eng. Fract. Mech. 200 (2018) 327–338, https://doi.org/10.1016/j.engfracmech.2018.08.004
[36] A.D. Evans, A. King, T. Pirling, G. Bruno, P.J. Withers, Near surface residual stress determination of laser shock peening by neutron diffraction, J. Neut. Res. 11 (2003) 229–233, https://doi.org/10.1080/10238160410001726606
[37] L. Lan, R. Xin, X. Jin, S. Gao, B. He, Y. Rong, N. Min, Effects of laser shock peening on microstructure and properties of Ti–6Al–4V titanium alloy fabricated via

selective laser melting, Materials 13 (2020) 3261, https://doi.org/10.3390/ma13153261
[38] X. Cao, W. He, B. Liao, G. He, Y. Jiao, D. Huang, S. Wang, Effect of TiN/Ti coating combined with laser shock peening pre-treatment on the fatigue strength of Ti-6Al-4V titanium alloy, Surf. Coat. Technol. 403 (2020) 126393, https://doi.org/10.1016/j.surfcoat.2020.126393
[39] H. Carreon, M.L. Carreon, M. Carreon-Garciduenas, Nondestructive magnetic monitoring of residual stresses in a medical Ti–6Al–4V–ELI alloy using a fluxgate sensor, Phys. Mesomech. 23 (2020) 160–166, https://doi.org/10.1134/S1029959920020071
[40] S.A. Martinez, S. Sathish, M.P. Blodgett, M.J. Shepard, Residual stress distribution on surface-treated Ti-6Al-4V by X-ray diffraction, Exp. Mech. 43 (2003) 141–147, https://doi.org/10.1007/BF02410495
[41] B. Lin, C. Lupton, S. Spanrad, J. Schofield, J. Tong, Fatigue crack growth in laser-shock-peened Ti–6Al–4V aerofoil specimens due to foreign object damage, Int. J. Fatigue 59 (2014) 23–33, https://doi.org/10.1016/j.ijfatigue.2013.10.001
[42] S. Srinivasan, D.B. Garcia, M.C. Gean, H. Murthy, T.N. Farris, Fretting fatigue of laser shock peened Ti–6Al–4V, Trib. Int. 42 (2009) 1324–1329, https://doi.org/10.1016/j.triboint.2009.04.014
[43] X. Jin, L. Lan, S. Gao, B. He, Y. Rong, Effects of laser shock peening on microstructure and fatigue behavior of Ti–6Al–4V alloy fabricated via electron beam melting, Mater. Sci. Eng. A 780 (2020) 139199, https://doi.org/10.1016/j.msea.2020.139199
[44] F. Fomin, B. Klusemann, N. Kashaev, Surface modification methods for fatigue properties improvement of laser-beam-welded Ti-6Al-4V butt joints, Proc. Struct. Integ. 13 (2018) 273–278, https://doi.org/10.1016/j.prostr.2018.12.046
[45] C.N. Pintado, J. Vazquez, J. Dominguez, A. Perinan, M.H. Garcia, F. Lasagni, S. Bernarding, S. Slawik, F. Mucklich, F. Boby, and L. Hackel, Effect of surface treatment on the fatigue strength of additive manufactured Ti6Al4V alloy, Frattura ed Integrita Strutturale 14 (2020), 337–344; https://doi.org/10.3221/IGF-ESIS.53.26.
[46] I. Yeo, S. Bae, A. Amanov, S. Jeong, Effect of laser shock peening on properties of heat-treated Ti–6Al–4V manufactured by laser powder bed fusion, Int. J. Precis. Eng. Manuf. -Green. Tech.. 8 (2021) 1137–1150, https://doi.org/10.1007/s40684-020-00234-2
[47] X.D. Ren, W.F. Zhou, F.F. Liu, Y.P. Ren, S.Q. Yuan, N.F. Ren, S.D. Xu, T. Yang, Microstructure evolution and grain refinement of Ti-6Al-4V alloy by laser shock processing, Appl. Surf. Sci. 363 (2016) 44–49, https://doi.org/10.1016/j.apsusc.2015.11.192
[48] W. Zhou, X. Ren, F. Liu, Y. Ren, L. Li, Nanocrystallization in the duplex Ti-6Al-4V alloy processed by multiple laser shock peening, Metals 6 (2016) 297–306, https://doi.org/10.3390/met6120297
[49] H. Lu, Z. Wang, J. Cai, X. Xu, K. Luo, L. Wu, J. Lu, Effects of laser shock peening on the hot corrosion behaviour of the selective laser melted Ti6Al4V titanium alloy, Corr. Sci. 188 (2021) 109558, https://doi.org/10.1016/j.corsci.2021.109558
[50] I. Altenberger, E.A. Stach, G. Liu, R.K. Nalla, R.O. Ritchie, An in situ transmission electron microscope study of the thermal stability of near-surface microstructures induced by deep rolling and laser-shock peening, Scr. Mater. 48 (2003) 1593–1598, https://doi.org/10.1016/S1359-6462(03)00143-X
[51] R. Fabbro, P. Peyre, L. Berthe, X. Scherpereel, Physics and applications of laser-shock processing, J. Laser Appl. 10 (1998) 265–279, https://doi.org/10.2351/1.521861
[52] L. Berthe, R. Fabbro, P. Peyre, E. Bartnicki, Experimental study of the transmission of breakdown plasma generated during laser shock processing, Eur. Phys. J. Appl. Phys. 3 (1998) 215–218, https://doi.org/10.1051/epjap:1998222
[53] S. Keller, S. Chupakhin, P. Staron, E. Maawad, N. Kashaev, B. Klusemann, Experimental and numerical investigation of residual stresses in laser shock peened AA2198, J. Mater. Proc. Technol. 255 (2018) 294–307, https://doi.org/10.1016/j.jmatprotec.2017.11.023
[54] E837–08, *Standard test method for determining residual stresses by the hole-drilling strain-gage method. Standard tests method E837–08*, American society for testing and materials, West Conshohocken, PA, USA (2008).
[55] M. Steinzig, E. Ponslet, Residual stress measurement using the hole drilling method and laser speckle interferometry: Part 1, Exp. Tech. 27 (2003) 43–46, https://doi.org/10.1111/j.1747-1567.2003.tb00114.x
[56] M.F. Ashby, The deformation of plastically non-homogeneous materials, Philos. Mag. 21 (1970) 399–424, https://doi.org/10.1080/14786437008238426
[57] M.B. Toparli, M.E. Fitzpatrick, Effect of overlapping of peen spots on residual stresses in laser-peened aluminium sheets, Metall. Mater. Trans. 50A (2019) 1109–1112, https://doi.org/10.1007/s11661-018-05100-0
[58] Z. Kallien, S. Keller, V. Ventzke, N. Kashaev, B. Klusemann, Effect of laser peening process parameters and sequences on residual stress profiles, Metals 9 (2019) 655, https://doi.org/10.3390/met9060655
[59] S. Chupakhin, N. Kashaev, N. Huber, Effect of elasto-plastic material behavior on determination of residual stress profiles using the hole drilling method, J. Strain Anal. Eng. Des. 51 (2016) 572–581, https://doi.org/10.1177/0309324716663940